ACS OMEGA

Article

Cite This: ACS Omega 2019, 4, 8707−8719

http://pubs.acs.org/journal/acsodf

Highly Drug-Resistant HIV-1 Protease Mutant PRS17 Shows Enhanced Binding to Substrate Analogues

Johnson Agniswamy,[†] Daniel W. Kneller,[†] Rowan Brothers,[‡] Yuan-Fang Wang,[†] Robert W. Harrison,[§] and Irene T. Weber*[,†,‡]

[†]Department of Biology, Georgia State University, P.O. Box 4010, Atlanta, Georgia 30302, United States

[‡]Department of Chemistry, Georgia State University, P.O. Box 3965, Atlanta, Georgia 30302, United States

[§]Department of Computer Science, Georgia State University, P.O. Box 5060, Atlanta, Georgia 30302, United States

ABSTRACT: We report the structural analysis of highly drug-resistant human immunodeficiency virus protease (PR) variant PR^{S17}, rationally selected by machine learning, in complex with substrate analogues. Crystal structures were solved of inhibitor-free inactive PR^{S17}-D25N, wild-type PR/CA-p2 complex, and PR^{S17} in complex with substrate analogues, CA-p2 and p2-NC. Peptide analogues p2-NC and CA-p2 exhibit inhibition constants of 514 and 22 nM, respectively, for PR^{S17} or approximately 3-fold better than for PR. CA-p2 is a better inhibitor of PR^{S17} than are clinical inhibitors (K_i = 50−8390 nM) except for amprenavir (K_i = 11 nM). G48V resistance mutation induces curled flap tips in PR^{S17}-D25N structure. The inner P2−P2′ residues of substrate analogues in PR^{S17} complexes maintain similar conformations to those of wild-type complex, while significant conformational changes are observed in the peripheral residues P3, P4′ of CA-p2 and P3, P4, and P3′ of p2-NC. The loss of β-branched side chain by V82S mutation initiates a shift in 80's loop and reshapes the S3/S3′ subsite, which enhances substrate binding with new hydrogen bonds and van der Waals interactions that are absent in the wild-type structures. The steric hindrance caused by G48V mutation in the flap of PR^{S17} contributes to altered binding interactions of P3 Arg, P4′ norleucine of CA-p2, and P4 and P3′ of p2-NC with the addition of new hydrogen bonds and van der Waals contacts. The enhanced interaction of PR^{S17} with substrate analogues agrees with their relative inhibition, suggesting that this mutant improves substrate binding while decreasing affinity for clinical inhibitors.

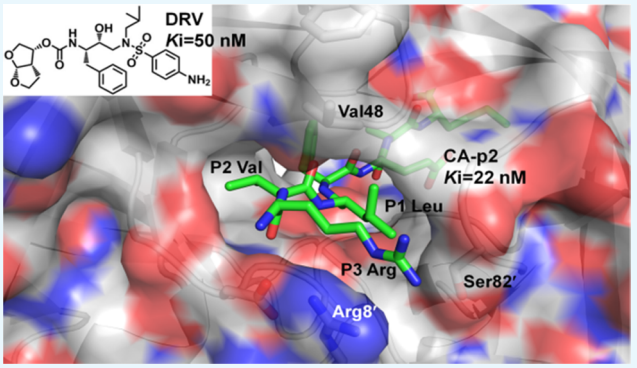

INTRODUCTION

Human immunodeficiency virus (HIV) currently infects approximately 36.7 million people worldwide. At present, there is no cure for HIV infection or AIDS.[1] However, the advent of combined antiretroviral therapy (cART) in the late 1990s using a combination of reverse transcriptase and protease (PR) inhibitors (PIs) dramatically suppressed the viral loads and increased CD4$^+$ T-cell counts among infected patients.[2,3] In addition to viral fusion to host cell, reverse transcriptase, and integrase, HIV protease (PR) is a critical antiretroviral drug target due to its pivotal role in the processing of Gag and Gag-Pol polyproteins during viral maturation. HIV PR is a homodimeric aspartic protease, in which each 99 amino acid monomer contributes one of the two catalytic triads (Asp25−Thr26−Gly27) required for catalytic function.[4] The Gag and Gag-pol polyproteins are processed by HIV PR at 10 sites by recognizing specific sequences of seven to eight residues at the cleavage site. The substrate residues at the cleavage site are numbered P4−P3−P2−P1−P1′−P2′−P3′−P4′ with the scissile peptide bond between P1 and P1′ residues. ^{18}O exchange mass spectrometry studies have shown that the peptide hydrolysis by HIV PR occurs through the formation of a reversible and metastable gem−diol reaction intermediate.[5] Several intermediates in the reaction pathway have been identified in X-ray crystal structures.[6] Inhibition of HIV PR leads to the disruption of the virus life cycle at a vital stage.[7] Currently, there are nine Food and Drug Administration (FDA)-approved PR inhibitors (PIs) that are available for cART. However, due to the rapid turnover rate of HIV and the low fidelity of reverse transcriptase (~2 × 10^{-5} errors/nucleotide per replication cycle), mutations in PR associated with resistance to each of the nine FDA-approved PIs have decreased the efficacy of current treatment options.[8,9] Accumulation of 10−20 mutations in PR may be required to evolve high levels of resistance.[10] Patients with multidrug-resistant HIV PR were shown to have convergently evolved patterns of accumulated resistance mutations.[11]

The recently studied HIV PR variant PR^{S17} has 17 mutations compared to the wild-type PR and was selected by mean-shift

Received: March 12, 2019
Accepted: May 7, 2019
Published: May 17, 2019

DOI: 10.1021/acsomega.9b00683
ACS Omega 2019, 4, 8707−8719

clustering on genotype−phenotype data using a new algorithm for predicting drug resistance with a unified encoding of the sequence and three-dimensional structure.[12,13] PR^{S17} was predicted to exhibit high-level resistance to six inhibitors: atazanavir, nelfinavir, ritonavir, indinavir, lopinavir, and saquinavir, and was subsequently confirmed to have resistance to eight of the nine currently available clinical inhibitors except for tipranavir, which could not be measured due to solubility limitations.[14,15] Structural studies using X-ray crystallography and NMR spectroscopy have shown that PR^{S17} exhibits an open-flap conformation in the absence of inhibitor in both crystal structure and in solution unlike the wild-type PR, which is present in the closed-flap conformation without the inhibitor in NMR studies.[16] In spite of different mutational profiles, correlated clusters of mutations in other multidrug-resistant variants of HIV PR (PR20 and MDR 769) cause them to also favor an open-flap conformation like PR^{S17} that lowers the binding affinity of inhibitors.[17,18] Altered dynamics of the flap due to mutations is likely to increase dissociation rates and, hence, decrease the potency of inhibitors.[19] Clusters of mutations at the hinge loop in PR^{S17} and PR20 are associated with increased flap dynamics and enhanced inhibitor dissociation of the two multidrug-resistant PRs.[16,17] These mutational clusters that function synergistically to produce conformational changes in the PR suggest convergent evolution by combinations of single mutations. Variant PR^{S17} is about 10-fold less efficient than the wild-type PR in processing the Gag polyprotein while maintaining the same order of substrate cleavage.[15] PR^{S17} is also 2-fold less efficient than PR20 in Gag polyprotein processing and forms an excellent prototype for structural studies on substrate binding to multidrug-resistant PR.

HIV PR hydrolyzes several sites with markedly different sequences on the nascent polyprotein substrate. In order for PR to evolve resistance to multiple drugs while maintaining catalytic efficiency for viral replication, mutations that destabilize inhibitor binding must combine with mutations that contribute to a new or altered form of substrate binding. This perspective shifts the focus of structure-guided drug design from point-based mutations to mutation clusters. Studying the mechanism by which multidrug-resistant variants like PR^{S17} bind and cleave substrates may elucidate conserved methods of binding across other mutant PRs with similar mutational clusters and give insights for improved structure-guided drug design. In the current study, we use structural and kinetic studies on PR, PR^{S17}-D25N, and PR^{S17} with substrate analogues CA-p2 (R-V-L-r-F-E-A-Nle) and p2-NC (Ace-T-I-Nle-r-Nle-Q-R) to evaluate differences in substrate recognition between PR^{S17} and wild-type PR. The reduced peptide analogues are suitable for structural studies with active PR variants since they cannot be hydrolyzed. Ace and the isosteric amino acid norleucine (Nle) in which the sulfur of the Met side chain is replaced by a methylene group were used to simplify the synthesis.

RESULTS

Substrate Analogue Inhibition of PR^{S17}. Gag cleavage sites p2-NC and CA-p2 are the first and last proteolytic sites to be processed in the Gag precursor.[20] Mutations accumulating near the p2-NC cleavage site have been shown to improve the processing fitness of a highly mutated HIV PR sequence isolated from a patient failing antiviral therapy.[21] Reduced peptide analogues corresponding to the amino acid sequence of Gag cleavage sites act as competitive inhibitors of HIV PR catalytic activity.[22−24] In the present study, reduced peptide analogues for p2-NC and CA-p2 cleavage sites inhibited the proteolytic activity of the drug-resistant HIV-1 PR mutant PR^{S17}. The k_{cat} and K_m values measured for PR^{S17} are 69.7 ± 14.4 min^{-1} and 143 ± 33.0 μM, respectively. The k_{cat}/K_m of PR^{S17} is 0.49 ± 0.05 min^{-1} μM^{-1}. Inhibition constants (K_i) measured for PR^{S17} were 514 nM for p2-NC and 22 nM for CA-p2. The inhibition constants (K_i) of substrate analogues for PR^{S17} are compared with the values for PR and PR^{V82A} determined previously in Table 1. Interestingly, reduced peptide analogue CA-p2 displays better inhibition values for PR^{S17} than those of clinical inhibitors (K_i = 50−8390 nM) except for amprenavir (APV) (K_i = 11 nM), as measured by isothermal titration calorimetry.[15] CA-p2 and p2-NC substrate analogues are 3.4 and 4.2-fold better inhibitors for PR^{S17}, respectively, when compared to PR whose K_i values are 75 nM and 2.17 μM. The major effect appears to be the mutation to a smaller side chain at Val82, since PR bearing single mutation V82A (PR^{V82A}) displays almost identical inhibition kinetics for CA-p2 (K_i = 24 nM) and p2-NC (K_i = 530 nM) as those measured for PR^{S17}.[24] PR^{S17} has a serine at this position, which is the only mutation in the active-site cavity apart from those in flaps.

Table 1. Inhibition Constants (K_i) in nM for PR, PR^{V82A}, and PR^{S17} [a]

protein	P2-NC	CA-p2
PR	2170	75
PR^{V82A}	530 (4.1)	24 (3.2)
PR^{S17}	514 (4.2)	22 (3.4)

[a]Values in parentheses are K_i values relative to the wild-type PR.

Overall Structure. Crystal structures of inhibitor-free PR^{S17}-D25N and wild-type PR in complex with CA-p2 substrate analogue were determined in the $P3_221$ and $P2_12_12$ space groups at 1.21 and 1.46 Å resolutions, respectively. PR^{S17} complex with CA-p2 crystallized in the monoclinic space group $P2_1$ and was refined to 1.7 Å, while PR^{S17} in complex with p2-NC was determined in two different space groups $P4_1$ and $P6_1$ at 1.71 and 1.67 Å resolutions, respectively. The five structures were refined to R-factors of 14.8−19.8%, as shown in the crystallographic statistics of Table 2. The inhibitor-free PR^{S17}-D25N structure has one monomer in the asymmetric unit with residues numbered 1−99, while PR/CA-p2, $PR^{S17-P41}$/p2-NC, and $PR^{S17-P61}$/p2-NC complexes contain a dimer of subunits numbered 1−99 and 1′−99′ in the asymmetric unit. The PR^{S17}/CA-p2 complex has two dimers per asymmetric unit. The substrate analogues bound at the active site in a single conformation in all PR and PR^{S17} complexes. All 17 mutations in the PR^{S17} (Figure 1A) and substrate analogues were unambiguously modeled in the electron density maps (Figure 1B,C). The reorganization of the hinge loop by mutations E35D, M36I, and S37D that breaks the ion pair anchoring the flaps and thereby increases the flap flexibility as described in the previously determined complex of PR^{S17} with darunavir (DRV)[16] is also observed in the current substrate analogue complexes.

Curling of Flaps in PR^{S17}-D25N. The current crystal structure of PR^{S17}-D25N at 1.21 Å is the highest-resolution HIV PR structure in the open conformation available to date. Comparison of inhibitor-free PR^{S17}-D25N with the wild-type

DOI: 10.1021/acsomega.9b00683
ACS Omega 2019, 4, 8707−8719

Table 2. Crystallographic Data and Refinement Statistics[a]

	PR^{S17}-D25N	PR/CA-p2	PR^{S17}/CA-p2	PR^{S17}/p2-NC	PR^{S17}/p2-NC
space group	$P3_221$	$P2_12_12$	$P2_1$	$P4_1$	$P6_1$
cell dimensions					
a (Å)	49.65	58.41	53.70	54.88	63.83
b (Å)	49.65	86.24	60.36	54.88	63.83
c (Å)	86.70	46.58	66.48	82.13	83.04
α (deg)	90	90	90	90	90
β (deg)	90	90	90.93	90	90
γ (deg)	120	90	90	90	120
resolution range (Å)	50.0−1.21 (1.25−1.21)	50.0−1.46 (1.51−1.46)	50.0−1.7 (1.76−1.70)	50.0−1.71 (1.77−1.71)	50−1.67 (1.73−1.67)
unique reflections	35 459 (1956)	38 064 (2696)	46 434 (4633)	26 117 (2508)	21 945 (1989)
redundancy	5.0 (2.1)	4.1 (1.7)	3.9 (3.8)	6.1 (3.4)	4.4 (2.3)
completeness	91.9 (52.1)	91.9 (66.5)	99.5 (99.6)	99.1 (95.2)	98.4 (89.2)
$\langle I/\sigma(I)\rangle$	18.7 (2.0)	11.0 (2.0)	17.1 (6.1)	21.2 (2.6)	16.9 (2.0)
R_{sym} (%)	7.1 (42.5)	9.0 (43.8)	7.6 (41.8)	7.1 (47.1)	5.7 (44.4)
refinement resolution range (Å)	50.0−1.21	50.0−1.46	34.53−1.7	27.46−1.71	33.22−1.67
R (%)	14.8	18.8	17.6	19.8	17.6
R_{free} (%)	16.4	24.5	21.2	23.1	21.6
number of atoms in asymmetric unit	920	1762	3416	1744	1804
number of water molecules	105	115	170	78	125
average B-factor (Å^2)					
main chain	18.6	15.7	18.0	39.1	28.6
side chain	23.3	21.1	23.8	44.9	35.1
inhibitor		26.2	19.6	37.9	25.4
waters	29.3	27.3	24.6	44.3	34.0
RMS deviations from ideality					
bond length (Å)	0.02	0.01	0.02	0.02	0.02
angles	1.8°	0.03 Å	2.2°	2.2°	2.2°

[a]Values in parentheses are for the highest shell.

PR open form without inhibitor (2PC0) shows that the two structures superpose with a root-mean-square deviation (RMSD) of 1.4 Å for the 99 topologically equivalent Cα atoms. The maximum deviation of 6.9 Å between the two structures occurs at Ile50 at the tip of the flap. Similar to the wild-type PR, the flaps of PR^{S17}-D25N are in an open conformation. The three mutations M46L, G48V, and I54V in PR^{S17} flaps act to curl the tip of flaps (Figure 2A). The twist in the flap starts at G48V of PR^{S17}-D25N with a drastic change in ϕ angle by ∼172° in comparison with Gly48 of the wild-type PR. The introduction of Val48 side chain in PR^{S17}-D25N results in ∼1.1 Å shift of Phe53 side chain's benzene ring when compared to that of the wild-type PR. This shift results in the loss of van der Waals contacts observed in the wild-type PR between the side chain of Phe53 and Gly48. In addition to the shift in Phe53, the mutation of Met46 to shorter Leu46 in PR^{S17}-D25N also eliminates van der Waals contacts observed in the wild-type PR between Phe53 and Met46. This curling of flap tips propagates from G48V up to Gly52 in PR^{S17}-D25N. As a result, the tip of the flap of PR^{S17}-D25N moves ∼4.4 Å closer to 80's loop, as measured by the distance between the Cα atoms of Ile50 and Thr80. This distance is 14.5 Å for the wild-type PR, while it is 10.1 Å for the PR^{S17}-D25N structure. The residues in 80's loop play an important role in the binding of both substrate and inhibitors to PR. Conformational changes and shifts in the 80's loop due to resistant mutations can eliminate interactions with inhibitors in both single mutants of PR and variants with multiple mutations.[4,17,25]

On the other hand, the flap curling also increases by ∼1.4 Å, the distance between the flap tip of PR^{S17}-D25N and the active site, since the distance between the Cα atoms of Asp25 and Ile50 increased from 17.6 Å in the wild-type structure to 19.0 Å in PR^{S17}-D25N. Nearly identical curled flap conformation was seen in the recently reported inhibitor-free PR^{S17} structure.[16] The overall structure of PR^{S17}-D25N is very similar to the inhibitor-free PR^{S17} structure with an RMSD of 0.18 Å for 99 equivalent Cα atoms. The maximum deviation between the two structures occurs for residue Ile50 at the flap tip with an RMSD of 1.1 Å. Similar to PR^{S17}-D25N, the flap curling in PR^{S17} starts with ∼176° change in φ angle of G48V and ends at Gly52. However, the peptide bond between Ile50 and Gly51 is flipped in PR^{S17} structure in comparison to PR^{S17}-D25N (Figure 2B). This flipped peptide bond enables residue Ile50 at the flap tip of PR^{S17} to move closer to the 80's loop residue Thr81 (∼8.8 Å) than in PR^{S17}-D25N (10.1 Å), while the distance between catalytic Asp25/Asn25 and the flap tip Ile50 remains more or less the same between the two structures (18.7 Å for PR^{S17} and 19.0 Å for PR^{S17}-D25N). Both conformations of the peptide bond between Ile50 and Gly51 are observed in other PR structures, which suggest that it can exist in either conformation. Also, PR with individual mutations of M46L, G48V, and I54V in the flaps showed worse inhibition constants (K_i) for DRV and saquinavir relative to the wild-type PR.[26,27] Thus, identical curling of flaps in two independently determined structures of PR^{S17}-D25N and PR^{S17} strongly implies that the conformational changes are

DOI: 10.1021/acsomega.9b00683
ACS Omega 2019, 4, 8707−8719

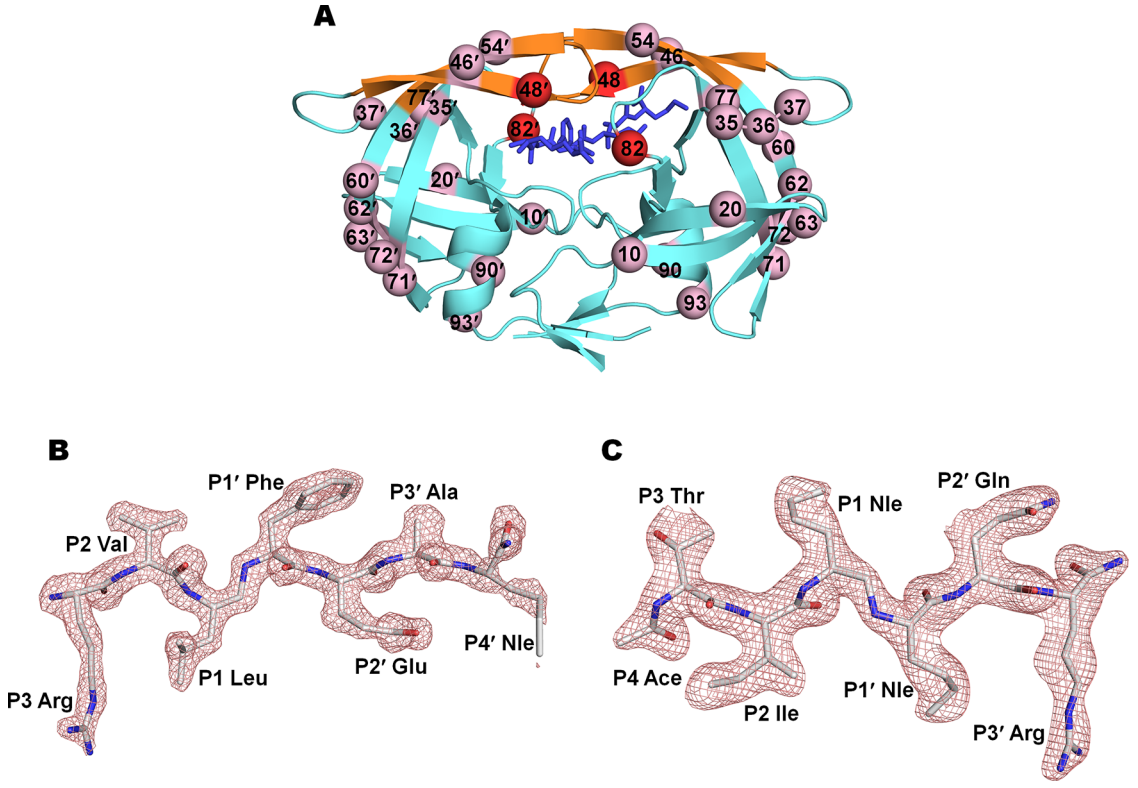

Figure 1. Sites of mutation in PR^{S17} dimer and substrate analogues. (A) Sites of 17 mutations are mapped on PR^{S17} dimer (cyan cartoon representation) with flap region in orange and bound substrate analogue CA-p2 shown as blue sticks. The critical G48V and V82S mutations involved in substrate analogue binding are shown as red spheres in each subunit. (B) F_o-F_c omit map of CA-p2 colored by element type contoured at 2.8σ level. (C) F_o-F_c omit map of p2-NC colored by element type contoured at 3σ level.

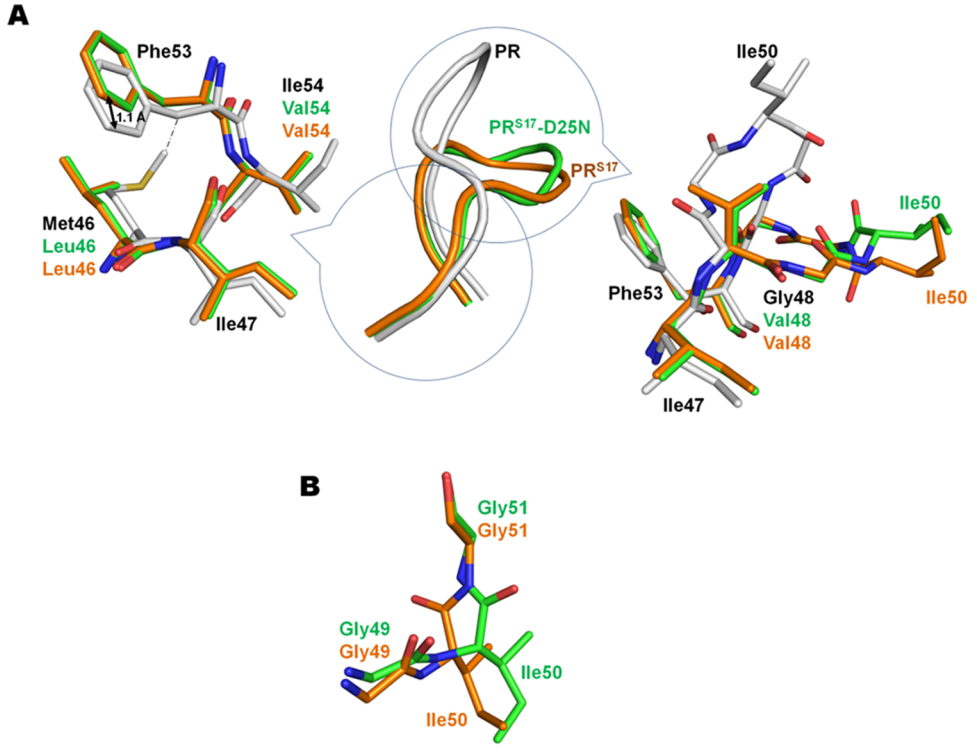

Figure 2. Altered flap of PR^{S17}-D25N. (A) Curling of the flap due to flap mutations M46L, G48V, and I54V observed in inhibitor-free structures of PR^{S17}-D25N (green ribbon) and PR^{S17} (orange ribbon) in comparison to PR (gray ribbon). The circled portions of the flap are magnified in sticks for inhibitor-free PR^{S17}-D25N (green carbon), PR^{S17} (orange carbon), and PR (gray carbon). (B) Flipped peptide bond between Ile50 and Gly51 of PR^{S17}-D25N (green carbon) and PR^{S17} (orange carbon).

DOI: 10.1021/acsomega.9b00683
ACS Omega 2019, 4, 8707−8719

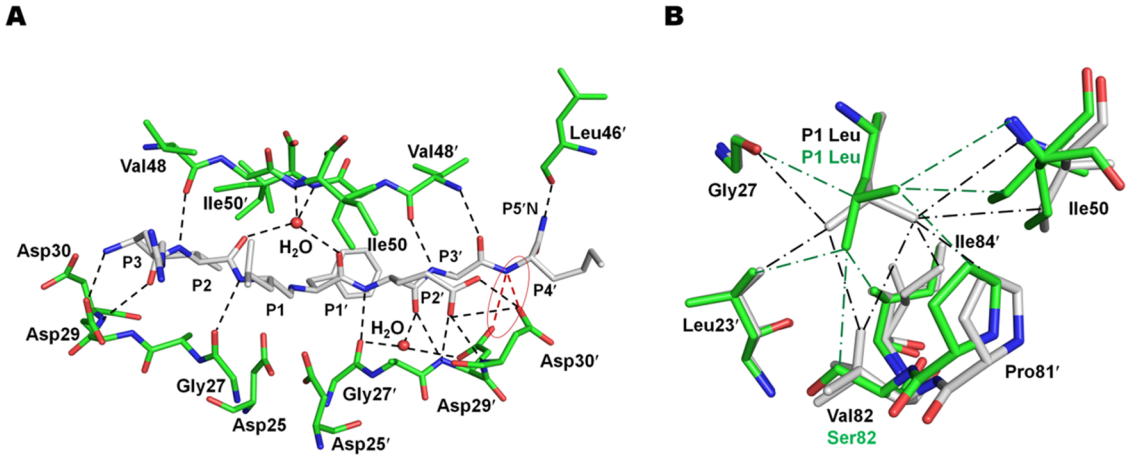

Figure 3. Overall interaction of substrate analogue CA-p2 with PR^{S17}. (A) Hydrogen bond interactions between PR^{S17} (green carbon) and substrate analogue CA-p2 (gray carbon). Water molecules are shown as red spheres in this and subsequent figures. Hydrogen bonds are shown in black dotted lines, and the new hydrogen bond observed between PR^{S17} and CA-p2 is shown in red dotted line. (B) Comparison of CA-p2 P1 Leu interaction in PR^{S17}/CA-p2 (green carbon) and PR/CA-p2 (gray carbon). The van der Waals contacts are represented by (– · – · –) lines in green in PR^{S17}/CA-p2 and in black in the PR/CA-p2 complex.

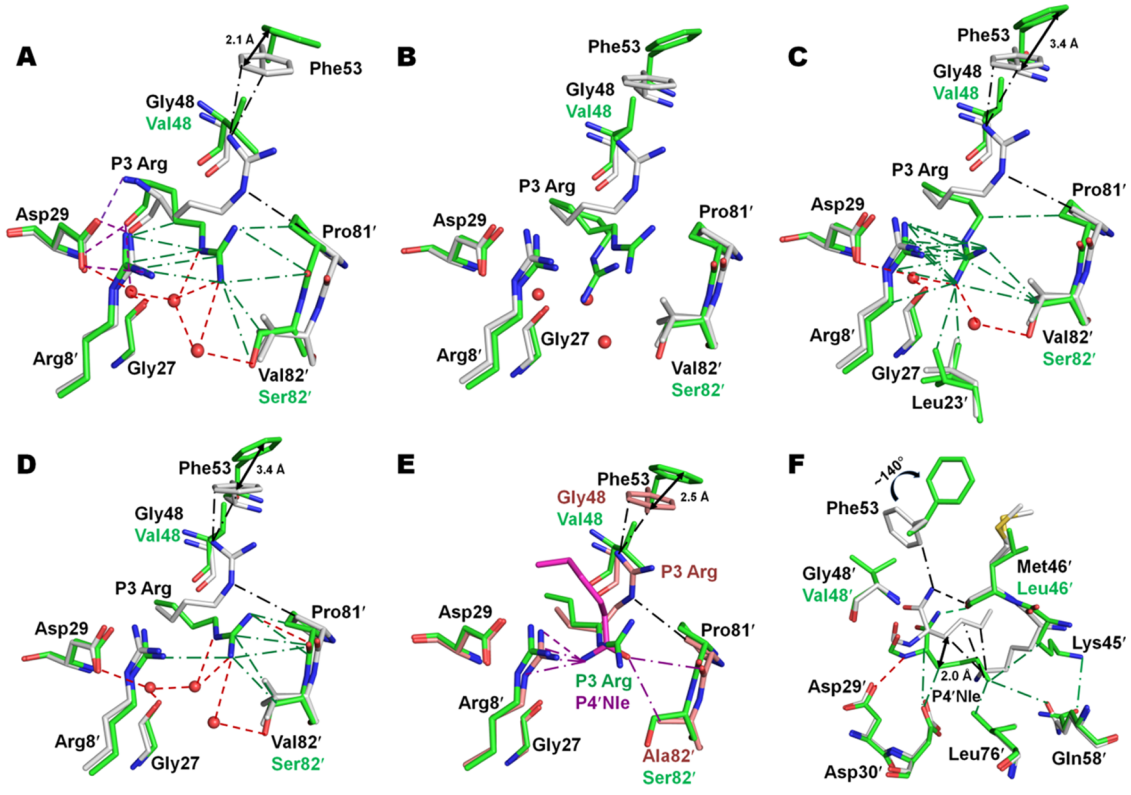

Figure 4. Interactions of P3 and P4′ of substrate analogue CA-p2 with PR^{S17}. (A) Interaction of P3 Arg of CA-p2 (conformation 1) in dimer 1 of PR^{S17}/CA-p2 (green carbon) and PR/CA-p2 (gray carbon). The hydrogen bonds common to both the complexes are shown in purple dotted lines. In all subpanels, new hydrogen bonds observed in the PR^{S17}/CA-p2 complex are shown in red dotted lines. The van der Waals contacts are represented by (– · – · –) lines in green in PR^{S17}/CA-p2 and in black in the PR/CA-p2 complex. (B) P3 Arg of CA-p2 (conformations 2 and 3) in dimer 2 of PR^{S17}/CA-p2 (green carbon). Interactions of conformations 2 and 3 are shown in panels (C) and (D), respectively. (C) Interactions of P3 Arg conformation 2 in dimer 2 of PR^{S17}/CA-p2 (green carbon) in comparison to PR/CA-p2 (gray carbon). (D) Interactions of P3 Arg conformation 3 in dimer 2 of PR^{S17}/CA-p2 (green carbon) in comparison to PR/CA-p2 (gray carbon). (E) Interactions of major conformation P3 Arg (salmon carbon) and minor conformation P4′ Nle (magenta carbon) of V82A single mutant complex PR^{V82A}/CA-p2 in comparison to PR^{S17}/CA-p2 (green carbon). The van der Waals contacts of P3 Arg of PR^{V82A}/CA-p2 are shown in black, while those of P4′ Nle are shown in magenta. (F) Difference in the binding of P4′ Nle between PR/CA-p2 dimer 1 (gray carbon) and PR^{S17}/CA-p2 (green carbon). The hydrogen bond present only in PR^{S17}/CA-p2 is colored in green, and the hydrogen bond present in the PR/CA-p2 complex alone is shown in black dotted lines.

due to the three mutations M46L, G48V, and I54V in the flaps of PR^{S17} and contribute to the altered kinetic characteristics of PR^{S17}.

PR^{S17} Recognition of the P2, P1′–P3′ Groups of CA-p2 Is Unaffected by the Resistance Mutations. The PR^{S17}/CA-p2 structure has two PR dimers in the asymmetric

DOI: 10.1021/acsomega.9b00683
ACS Omega 2019, 4, 8707–8719

unit. The two dimers agree well and can be superposed with an RMSD of 0.78 Å for the 198 canonically equivalent Cα atoms. Comparison of the two dimers in PR^{S17}/CA-p2 structure with the wild-type PR/CA-p2 complex with one dimer in the asymmetric unit shows RMSDs of 1.05 and 0.71 Å, respectively, for each dimer. The maximum deviation of 4.4 Å occurs between residues Glu35′ of PR/CA-p2 and PR^{S17}/CA-p2 in dimer 1, while 4.3 Å deviation is observed between Glu35 positions in dimer 2. PR forms a series of hydrogen bond interactions with the main-chain amide and carbonyl of the substrate that are important for the recognition of peptides.[24] Similar hydrogen bonds between the main chains of PR and substrate analogue were observed in both the PR/CA-p2 and PR^{S17}/CA-p2 complexes (Figure 3A), except for a new longer hydrogen bond between the main-chain amide of P4′ Nle and the side chain of Asp29′ or Asp30′ in the PR^{S17}/CA-p2 complex, which will be discussed in a later section. The conformations of P2 Val, P1′ Phe, P2′ Glu, and P3′ Ala of CA-p2 and their interactions with the wild-type PR and PR^{S17} are similar in both complexes. However, conformational differences in P1 Leu, P3 Arg, and P4′ Nle of CA-p2 and variations in their interaction with PR residues are observed between the PR/CA-p2 and PR^{S17}/CA-p2 complexes.

The P1 Leu of PR/CA-p2 forms van der Waals interactions with the β-branched aliphatic side chain of Val82′. In the PR^{S17}/CA-p2 complex, Val82 is mutated to polar Ser82, which alters the size of the S1 pocket where P1 Leu binds. The P1 Leu side chain in PR^{S17}/CA-p2 is rotated by ∼46° about the χ^2 angle in comparison to its conformation in the wild-type complex, thus enabling P1 Leu to retain its van der Waals interaction with the side chain of V82′S in PR^{S17} (Figure 3B). The conformational change in the side chain of P1 Leu also facilitates the retention of van der Waals contacts with Leu23′, Gly27, Ile50, Pro81′, and Ile84′ observed in the PR/CA-p2 complex (Figure 3B). The P1 Leu of CA-p2 in the second dimer of the PR^{S17}/CA-p2 complex exhibits an identical conformation change with ∼46° rotation about χ^2 angle and retention of van der Waals contact with V82′S side chain, which further confirms that the observed change in P1 Leu of CA-p2 occurs in response to V82′S mutation in PR^{S17}.

Altered Recognition of CA-p2 P3 Arg Modulated by V82S Mutation. The P3 Arg main chain of PR/CA-p2 is fixed in position by the hydrogen bond between the N-terminal group of P3 and the side chain of Asp29 and a second hydrogen bond between the main-chain carbonyl of P3 Arg and the main-chain amide of Asp29. These two hydrogen bonds between Asp29 and the main chain of P3 Arg are also present in the PR^{S17}/CA-p2 complex (Figure 4A). The side chain of P3 Arg in the wild-type complex extends over the Gly48 in the first strand of the flap and forms van der Waals contacts with the Phe53 side chain in the second strand of the flap. In PR^{S17}, the Val side chain of G48V mutation produces steric hindrance and prevents the formation of the interaction between Phe53 and P3 Arg observed in the wild-type PR complex. The tip of Phe53 benzene ring in PR^{S17}/CA-p2 moves away by more than 2 Å in comparison to the wild-type complex. In the PR^{S17}/CA-p2 complex, P3 Arg is observed in three different conformations. Conformation 1 is in dimer 1 of the PR^{S17}/CA-p2 complex, while conformations 2 and 3 of P3 Arg are present as alternate conformations of 0.5 occupancy each in dimer 2 of the PR^{S17}/CA-p2 complex. Due to the steric hindrance caused by G48V mutation, all three conformations of the side chain of P3 Arg in PR^{S17}/CA-p2 dimers swing away from Val48 and interact with Arg8′. The inter-subunit ion pair formed by Arg8′ and Asp29 is critical for the dimer stability of HIV PR.[28] PR^{S17} utilizes both residues involved in this conserved ion pair to recognize and position P3 residue of CA-p2 substrate.

The new conformation of P3 Arg forms additional van der Waals contacts with Arg8′, Val48, Pro81′, and Ser82′ in PR^{S17} relative to those observed in the wild-type complex (Figure 4A). Also, the new orientation of P3 Arg guanidine head forms water-mediated hydrogen bonds with the hydroxyl side chain of Ser82′, which stabilizes the conformation of P3 Arg. Further, the guanidine head of P3 Arg in PR^{S17}/CA-p2 forms a double water-mediated hydrogen bond with the carbonyl oxygen of catalytic triad residue Gly27 and Asp29. These internal structural waters are highly conserved in most HIV PR structures, including the wild-type PR/CA-p2 complex. Similar interactions are also observed for conformations 2 and 3 of P3 Arg in the second dimer of PR^{S17}/CA-p2 (Figure 4B). In conformation 2, the guanidine of P3 Arg forms stacking interaction with Arg8′ (Figure 4C), while the guanidine of P3 Arg in conformation 3 forms van der Waals interaction with Arg8′ and hydrogen bond interaction with the main-chain carbonyl oxygen of Pro81′ (Figure 4D). The P3 Arg conformation 3 in dimer 2 forms fewer van der Waals contacts to Arg8′ than seen for conformation 1 in dimer 1. The guanidine head of P3 Arg in conformation 2 is buried deep in the pocket and forms additional van der Waals contacts with Leu23′ that are not present in conformation 1 or 3. This conformation is further held in place by a single water-mediated hydrogen bond between P3 Arg guanidine head and Asp29, as well as another one to the main-chain carbonyl of catalytic triad residue Gly27 of PR^{S17}. In contrast, conformation 3 forms double water-mediated hydrogen bonds with Gly27 and Asp29. The guanidine head of both conformations 2 and 3 of P3 Arg in dimer 2 has a water-mediated hydrogen bond to the hydroxyl of Ser82′, which further anchors P3 Arg of substrate analogue. The V82′S mutation in PR^{S17} facilitates the new conformation of P3 Arg side chain, since Val82′ in the wild-type complex would sterically interfere with P3 Arg in this location. Mutations of Val82 to Ala, Thr, Phe, Ile, Ser, and Leu are associated with resistance to clinical HIV PR inhibitors.[9,29] Similar to V82S mutation in PR^{S17}, V82A mutation is also expected to expand the binding site for P3 Arg, but other larger and β-branched mutations may block the access to this site. The co-occurrence of flap mutations like G48V that block P3 substrate-binding site and large substitutions at residue 82 like V82F, V82L, and V82I that block the alternate P3 binding site are expected to be detrimental to PR activity. In the previously solved crystal structure of PR^{V82A}/CA-p2, the substrate analogue is in two alternate conformations related by 180° with 0.65/0.35 occupancies as opposed to a single conformation in the current PR and PR^{S17} complexes. The major conformation of P3 Arg in the PR^{V82A}/CA-p2 complex forms van der Waals contact with Phe53 in the second strand of the flaps similar to the PR/CA-p2 complex, while the carbonyl of P4′ Nle of the minor conformation related by 180° occupies the P3 Arg site observed in the PR^{S17}/CA-p2 complex (Figure 4E). Similar to V82S, V82A mutation opens up the S3 site for substrate recognition. Thus, in the PR^{S17}/CA-p2 complex, the G48V flap mutation in conjunction with the V82S mutation facilitates the binding of the side chain of P3 Arg in the new site. The effect of Val82 mutation appears to be two-fold; it alters the

DOI: 10.1021/acsomega.9b00683
ACS Omega 2019, 4, 8707−8719

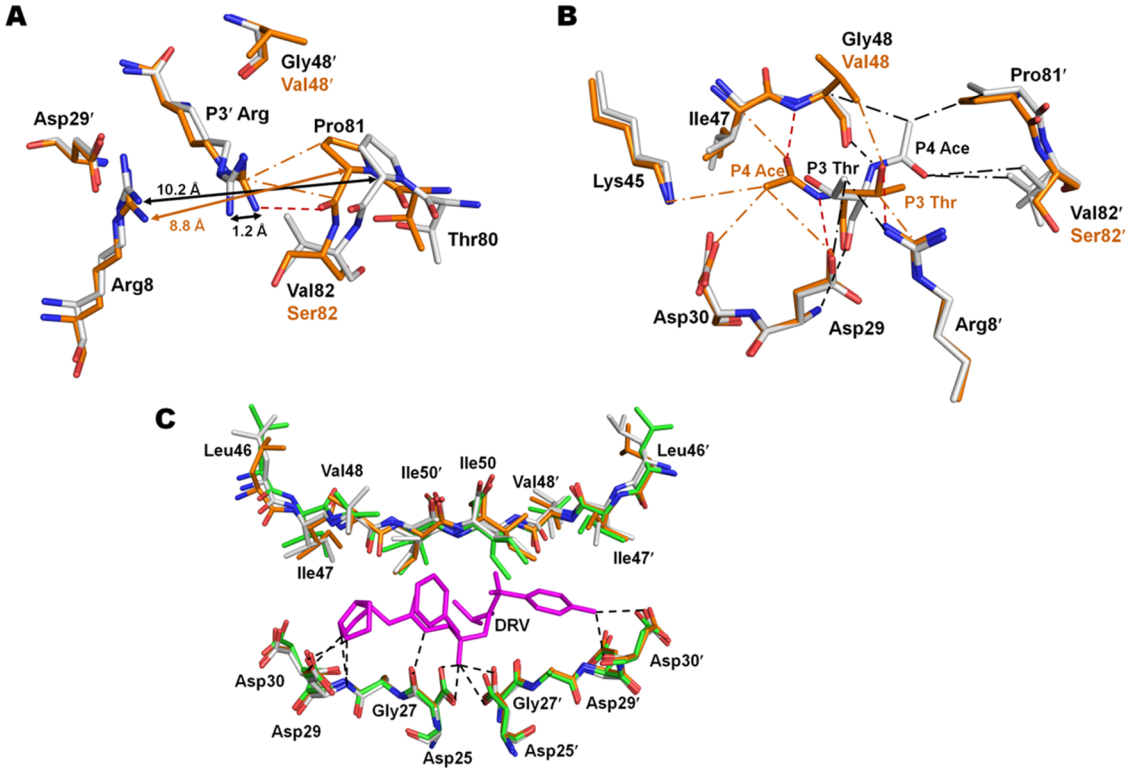

Figure 5. Binding of P3′, P3, and P4 residues of p2-NC and DRV to PR^{S17}. (A) P3′ Arg forms new hydrogen bond and van der Waals contacts colored in red with Pro81 of PR^{S17}/p2-NC (orange carbon) in comparison to PR/p2-NC (gray carbon, 2AOD). (B) Difference in P3 Thr interactions between PR^{S17}/p2-N (orange carbon) and PR/p2-NC (gray carbon). The three new hydrogen bonds observed in PR^{S17}/p2-NC are colored in red. The minor conformation of Arg8′ observed in PR/p2-NC was omitted for clarity. The van der Waals lines in this panel show residues in contact and may have more than one interaction between the residues. (C) Superposition of the active-site cavity of PR^{S17}/CA-p2 (green carbon), $PR^{S17\text{-}P41}$/p2-NC (orange carbon), and PR^{S17}/DRV (gray carbon, 5T2Z). DRV bound at the active site is shown in magenta sticks. The hydrogen bond interactions between DRV and PR^{S17} are shown in dotted lines. For the sake of clarity, water-mediated hydrogen bonds between DRV and the flaps are omitted.

resistance profile of PR inhibitors and regulates the access to Arg8/8′ in the recognition of substrate P3 residue in response to resistance flap mutations like G48V that hinder substrate recognition.

Effects of G48′V Mutation on Binding of CA-p2 P4′ Nle to Leu76′ Hydrophobic Pocket. Comparison of PR and PR^{S17} complexes with CA-p2 reveals significant differences in the binding of P4′ Nle. In the wild-type PR/CA-p2 complex, the terminal P5′ NH_2 group forms a hydrogen bond interaction with the main-chain carbonyl of Leu46 and van der Waals interactions with Phe53 in the second strand of the flap (Figure 4F). However, in the mutant PR^{S17}/CA-p2 complex, the introduction of G48V mutation causes the Phe53 side chain to rotate out by more than 140° in comparison to the wild-type complex. The G48V mutation further contributes to more than 1.5 Å shift in the position of terminal P5′ NH_2, which loses van der Waals contact with Phe53 but retains the hydrogen bond with the carbonyl of Leu46. The main-chain amide of P4′ Nle is moved by ∼0.8 Å in the PR^{S17}/CA-p2 complex in comparison to that in the wild-type complex, which results in a new long hydrogen bond (∼3.5 vs ∼4.1 Å in the PR/CA-p2 complex) between the main-chain amide of P4′ Nle and the side chain of Asp29′ in dimer 1. P4′ Nle amide in dimer 2 forms a water-mediated hydrogen bond with Asp29′ and a new long hydrogen bond with the side chain of Asp30′ (∼3.5 vs ∼3.8 Å). The Cα atom of P4′ Nle is also shifted by ∼1.2 and 0.5 Å in comparison to its position in PR/CA-p2 in dimers 1 and 2, respectively. Along with the shift in the main-chain atoms, the side chain of P4′ Nle in dimer 1 swings into the hydrophobic pocket around Leu76′ and forms a hydrophobic interaction with the side chain of Leu76′. The side chain of Lys45′, which occupies this pocket and has van der Waals contacts with Asp30′ in the wild-type PR/CA-p2 structure, swings away to form a van der Waals interaction with the Gln58′ side chain in the PR^{S17}/CA-p2 complex, thereby enabling P4′ Nle of CA-p2 to interact with Leu76′. P4′ Nle bound in this pocket also forms van der Waals interactions with Asp30′, Lys45′, and Gln58′ in the mutant. In contrast, the P4′ Nle side chain in wild-type complex shows van der Waals contact with only one residue, Lys45′. The P4′ Nle side chain in the second dimer of PR^{S17}/CA-p2 also binds in the same pocket with similar interactions due to the G48′V flap mutation in PR^{S17}. Thus, the G48′V mutation in the flap and the altered conformation of Phe53′ in the PR^{S17}/CA-p2 complex induce a shift in P4′ Nle side chain away from the flaps to form a new hydrogen bond with Asp29′ or Asp30′. Further, the side chain of P4′ Nle in the new orientation binds in the hydrophobic pocket near Leu76′ with added van der Waals contacts. Overall, this new arrangement in the mutant confers favorable interactions with P4′ Nle.

Mutation V82S Mediates Enhanced Binding of P3′ Arg in p2-NC. PR^{S17} in complex with p2-NC was crystallized in two different space groups $P4_1$ and $P6_1$ and refined to resolutions of 1.71 and 1.67 Å, respectively. Both structures have one PR^{S17} dimer per asymmetric unit and a single conformation of substrate analogue bound at the active-site

DOI: 10.1021/acsomega.9b00683
ACS Omega 2019, 4, 8707−8719

cavity. The two structures are very similar with an RMSD of 0.5 Å for 198 equiv Cα atoms. The previously solved PR/p2-NC complex can be superposed with the $PR^{S17-P41}$/p2-NC and $PR^{S17-P61}$/p2-NC complexes with RMSD values of 0.99 and 0.96 Å, respectively, for the 198 equivalent Cα atoms. Despite their different space groups, both structures exhibit a maximum deviation of more than 4.3 Å at the same residue, Asp35, in comparison to the wild-type structure. The conformation of P2, P1, P1′, P2′, and P4′ residues of p2-NC and their interactions with PR^{S17} residues are similar for the PR^{S17}/p2-NC complexes in the two space groups and PR/p2-NC. However, noticeable differences occur at residues P3′, P3, and P4 of $PR^{S17-P41}$/p2-NC and $PR^{S17-P61}$/p2-NC in comparison to PR/p2-NC.

Unlike the P3 Arg of the PR/CA-p2 complex, the P3′ Arg of PR/p2-NC binds in the space between Arg8 and Val82 (Figure 5A). The side chain of P3′ Arg forms van der Waals contacts with Arg8 and the Cδ2 side-chain atom of Val82. In both $PR^{S17-P41}$/p2-NC and $PR^{S17-P61}$/p2-NC complexes, the P3′ Arg binds in the same pocket albeit the guanidine head of P3′ Arg is tilted toward V82S mutation due to the lack of a β-branched Cδ atom in residue 82. The Nε2 atom of the guanidine head of P3′ Arg in PR^{S17} complexes is shifted by 1.0 Å ($PR^{S17-P41}$/p2-NC) and 1.2 Å ($PR^{S17-P61}$/p2-NC) toward V82S in comparison to the PR/p2-NC complex. The loss of β-branched side chain in V82S mutation results in a significant shift of 80's loop residues toward Arg8 in PR^{S17} complexes. The Cα atoms of residues Thr80, Pro81, and V82S are shifted by 1.1, 1.3, and 0.7 Å, respectively, for the $PR^{S17-P41}$/p2-NC complex and 1.3, 1.4, and 0.6 Å for the $PR^{S17-P61}$/p2-NC complex from the corresponding Cα atoms in the PR/p2-NC complex (Figure 5A). This shift contracts the binding pocket for P3′ Arg of p2-NC by 1.3 and 1.4 Å, as measured by the distance between the guanidine head Nη1 of Arg8 and the Cα atom of Pro81, in $PR^{S17-P41}$/p2-NC and $PR^{S17-P61}$/p2-NC in comparison to the wild-type complex. This narrowing of the pocket results in the enhanced binding of P3′ Arg as it is able to form a new hydrogen bond interaction with the main-chain carbonyl of Pro81 in addition to van der Waals interactions with the side chain of Pro81 in the PR^{S17}/p2-NC complexes. In contrast, P3′ Arg in the wild-type PR/p2-NC complex has no interaction with Pro81. Both mutant PR^{S17}/p2-NC complexes retain the extensive van der Waals contacts between the Arg8 of PR^{S17} and P3′ Arg of substrate analogue seen in the wild-type complex. Similar shifting of 80's loop residues is also observed in the P3 pocket of both dimers of the PR^{S17}/CA-p2 complex in comparison to the wild-type structure, although the shifts are reduced by half ranging from 0.3 to 0.5 Å, likely due to the two alternate conformations of P3 Arg bound in this pocket. Thus, the analysis of the three PR^{S17} substrate analogue complexes indicates that the loss of β-branched side chain by V82S mutation initiates the shifting of 80's loop and reshapes the S3/S3′ subsite for enhanced binding and interactions with P3/P3′.

G48V Mutation of PR^{S17} Results in Altered Binding Position of P3 and P4 Residues of p2-NC and Addition of Two New Hydrogen Bonds. The P3 Thr in both $PR^{S17-P41}$/p2-NC and $PR^{S17-P61}$/p2-NC complexes exhibits significant structural changes in comparison to the wild-type complex. The p2-NC main-chain carbonyl oxygen of P3 Thr occupies identical positions in all three structures. The hydrogen bond observed between the P3 carbonyl and the main-chain amide of Asp29 in the PR/p2-NC complex, as well as the conserved water-mediated hydrogen bonds between the P3 carbonyl and Gly27 and Asp29, is preserved in both PR^{S17}/p2-NC complexes. However, the larger G48V mutation in PR^{S17} complexes induces shifts in P3 Thr Cα and Cβ atoms by ∼0.7 and 1.8 Å in comparison to their corresponding positions in the PR/p2-NC complex (Figure 5B). In this new conformation, the P3 Thr side chain forms several van der Waals contacts with the side chains of G48V mutation and Arg8′ in PR^{S17} complexes. It also forms a hydrogen bond interaction with Arg8′ side chain in both the complexes. In contrast, P3 Thr side chain in the wild-type PR/p2-NC complex forms a lone van der Waals contact with Arg8′ side chain but no hydrogen bonds. In comparison to the wild-type complex, the main-chain amide nitrogen of P3 Thr in both PR^{S17}/p2-NC complexes is rotated about ∼160° along the main-chain Cα−C bond. This results in a shift of the amide nitrogen of P3 Thr in both mutant complexes by ∼2.8 Å from the corresponding position in the PR/p2-NC complex. The amide nitrogen of P3 Thr forms a hydrogen bond interaction with the carbonyl oxygen of Gly48 in the wild-type PR/p2-NC complex, while it interacts with the side chain of Asp29 in both PR^{S17}/p2-NC complexes.

The terminal P4 Ace residue of p2-NC exhibits the maximum deviations among the substrate analogue residues in both PR^{S17} complexes in comparison to PR/p2-NC. The P4 residue in the PR^{S17} cannot occupy the same pocket as in the wild-type structure due to steric hindrance from G48V mutation and the loss of interaction with Val82′ as a result of V82′S mutation. The P4 Cα is shifted by ∼4.6 Å in both complexes from its position in the wild-type complex. Due to G48V mutation inducing ∼160° of rotation along the Cα−C bond of P3 residue, the P4 Ace residue occupies a different binding pocket in PR^{S17} complexes to that observed in the wild-type structure. The P4 residue in the wild-type PR/p2-NC complex forms van der Waals contacts with Gly48, Gly49, Pro81, and Val82. In contrast, the P4 residue in the PR^{S17}/p2-NC complexes has van der Waals contacts with a different set of residues: Val48, Asp29, Asp30, Lys45, and Ile47. In addition, the main-chain carbonyl oxygen of the P4 residue in PR^{S17} complexes forms new hydrogen bond interaction with the main-chain amide of Val48. Thus, despite large shifts in P3 and P4 residues induced by the G48V mutation, PR^{S17} accommodates the substrate residues in alternate sites and gains two hydrogen bond interactions. The new hydrogen bonds observed in the PR^{S17}/p2-NC complexes likely contribute to the improved p2-NC substrate analogue inhibition constant observed for PR^{S17} compared to those in PR.

PR^{S17} Binds Substrate Analogues CA-p2, p2-NC, and Inhibitor DRV without Drastic Change in PR Conformation around the Active Site. The two dimers of the PR^{S17}/CA-p2 complex together with the $PR^{S17-P41}$/p2-NC and $PR^{S17-P61}$/p2-NC structures can be superposed with PR^{S17}/DRV complex with an RMSD of 0.4−0.7 Å. No dramatic changes are observed in the conformation of residues around the active-site catalytic triad and the binding of substrate analogues and inhibitor (Figure 5C). Most of the conformational changes are seen in the flap residues. The serine side chain of V82S mutation in both monomers of PR^{S17}/DRV has two alternate conformations mimicking the two β-branches of valine, while in the substrate analogue complexes, it has a single conformation that points away from Arg8 to accommodate the substrate residues. Side-chain rotamer

DOI: 10.1021/acsomega.9b00683
ACS Omega 2019, 4, 8707−8719

changes are observed in Phe53 and in mutated side chains of Leu46 and Val48 in complexes with DRV and the two substrate analogues. In addition, shifts are observed for flap residues. A shift of 0.8 Å in M46L is observed in PR^{S17}/CA-p2 in comparison to complex with DRV. Similarly, Val48 of PR^{S17} shifts by 0.6 Å when bound to p2-NC analogue in comparison to its position in the complex with DRV. Flap mutations M46L, G48V, and I54V in PR^{S17} are implicated in the curling of flaps observed in the inhibitor-free structure.[16] In PR^{S17}/DRV complex, M46L and G48V mutations are shown to synergistically alter the conformation of Phe53 by steric hindrance underlying the relationship between the three residues.[16] Through changes in the flap strands including the position of M46L or G48V in combination with the change in rotamer for side chains of Leu46, Val48, and Phe53, PR^{S17} binds substrate analogues as tightly as it binds DRV (K_i = 50 nM). The larger side chain of the G48V mutation in the S2 pocket may play an important role in the better inhibition constant (K_i = 11 nM) of APV for PR^{S17}. Thermodynamic integration and molecular mechanics Poisson−Boltzmann surface area studies have shown that the larger side chain introduced by G48V mutation strengthens van der Waals interactions with APV.[30] However, G48V together with M46L also alters the conformation of other flap residues like Phe53 as seen in PR^{S17}/DRV complex,[16] which may affect the inhibitor binding. Thus, minimal structural changes enable highly drug-resistant PR^{S17} to bind substrate analogues with similar affinity as for DRV and better than for the other clinical inhibitors, contributing to both viral fitness and drug resistance.

DISCUSSION

Our studies on PR^{S17} demonstrate the value of using machine learning on genotype−phenotype data to select informative mutants for further analysis. Among the 17 mutations in PR^{S17}, G48V and V82S play critical roles in the binding of CA-p2 and p2-NC substrate analogues. The active-site cavity around Val82 is important for the binding of PR substrates, as well as clinical inhibitors. Drug-resistant mutations of Val82 are reported for all clinical PR inhibitors except for DRV.[9] The side chains of mutations vary in size from the smaller V82A to bulkier V82F in addition to V82S, V82T, V82L, and V82I that are in between.[9] V82A is one of the earlier PR mutations to occur at the active site among patients undergoing antiviral therapy[31] and has been the best-studied mutation at position 82. Kinetic studies have shown that PR bearing the single V82A mutation has a significantly worse affinity for PR inhibitors indinavir, nelfinavir, ritonavir, and DRV, while smaller effects were seen for the cleavage of PR substrate.[32−35] Structural studies on V82A mutant in complexes with nelfinavir, indinavir, ritonavir, DRV, and saquinavir all reveal a small shift in residues to accommodate the inhibitor, explaining the cross-resistance profile of this mutation to all PR inhibitors.[36,37] Resistance mutations like V82A at the active site of HIV PR interfere with the binding of drugs; however, replication of the virus requires successful binding and hydrolysis of Gag and Gag-Pol substrates by resistant PR variants. Crystal structures of inactivated PR with active-site D25N and V82A mutations in complex with substrates CA-p2, p1-p6, and MA-CA show high structural similarity with inactivated PR-D25N/substrate complexes,[38] which indicates that V82A mutation in conjunction with active-site D25N does not affect substrate binding. However, mutations in the Gag substrate cleavage sites can coevolve with resistance-associated mutations in HIV PR or mutations that alter the fitness of HIV PR.[39−42] NC-p1 cleavage site, which is the rate-limiting step in Gag polyprotein processing,[43] has been reported to coevolve with Ala to Val mutation at the P2 position of the substrate in response to V82A-resistant mutation.[40,44,45]

Mutations in the flap region also alter the PR susceptibility to inhibitors. In particular, flap mutation G48V confers a high level of resistance to saquinavir.[46] G48V mutation is also selected by PR inhibitors atazanavir, indinavir, lopinavir, and nelfinavir.[46−48] G48M has a similar resistance profile as G48V.[46] Less prevalent resistance mutations G48A/S/T/Q are less well studied and their clinical significance is not fully understood.[49] Most of the Gly48 mutations occur in viruses with multiple PI-resistant sequences[49] like PR^{S17}. G48V is associated with V82A in saquinavir resistance[50,51] and this pair occurs as a mutational cluster together with nonactive-site mutant C95F, which emphasizes the importance of coevolution of mutations at 48 and 82 in drug resistance. Mutations at 48 and 82 together with those at 30, 84, and 90 are considered primary mutations that are necessary for inhibitor resistance.[52] The present structural study reveals that PR^{S17}, a multidrug-resistant PR harboring primary mutations at 48 and 82 in addition to others, recognizes substrate analogues CA-p2 and p2-NC in an altered fashion in comparison to wild-type structures. The crystal structure of unliganded PR^{S17}-D25N exhibits curling of flap tips in comparison to unliganded wild-type structure. This flap curling is initiated by G48V mutation with a ∼172° change in ϕ angle in comparison to PR wild type and extends up to Gly52′. In addition to G48V, other flap mutations M46L and I54V may also contribute to curling in PR^{S17}. Identical flap curling was observed in the recent unliganded PR^{S17} crystal structure.[16] Also, solution studies of PR^{S17}-D25N by NMR demonstrated that the inhibitor-free PR^{S17}-D25N adopts a flap conformation very similar to that of the inhibitor-free active PR^{S17} crystal structure. The current crystal structure of PR^{S17}-D25N further confirms that the conformation changes observed in the flaps of the two unliganded structures of PR^{S17} are due to the mutations. Curling or twisting of flaps in the PR structures due to mutations in the flaps is implicated in the altered resistance profile of the mutant PR. F53L single mutant, which exhibits curled flaps, was shown to possess a 15% lower catalytic efficiency and a 20-fold weaker inhibition by clinical drug indinavir.[53] Twisting of flaps observed in the recently reported PR with 22 mutations in addition to inactivating D25N mutation has >175-fold resistance to DRV in addition to APV.[54] The flap twisting initiated by G48V mutation in PR^{S17} is implicated in the cross-resistance of PR^{S17} to multiple clinical drugs including DRV even though it lacks any major mutations associated with DRV resistance.[16]

Although the binding site for P3 Arg of CA-p2 in the current PR/CA-p2 complex is partly exposed to solvent, P3 Arg interacts with flap residue Phe53 in a manner similar to that seen in the CA-p2 complexes with PR (4EP3), PR^{V82A} (2AOE), and inactive PR-$D25N^{V82A}$ (1MT8). With P3 Arg bound at the preferred wild-type flap-binding site, mutations at 82 with large side chains like V82F, V82I, or V82L hinder the binding of PR inhibitors, thereby altering PR susceptibility to PIs while retaining binding to substrates. The G48V mutation in PR^{S17} also confers resistance to PR inhibitors[16] and blocks the flap-binding site for P3 Arg of CA-p2 observed in the various wild-type PR complexes. However, V82/82′S mutation in PR^{S17} results in ∼1 Å shift in the residues of the 80's loop

DOI: 10.1021/acsomega.9b00683
ACS Omega 2019, 4, 8707−8719

and rearrangement of the S3/S3′ pocket between V82/82′S and the conserved Arg8′/8. Both P3 Arg of CA-p2 and P3′ Arg of p2-NC bind in this subsite of PR^{S17} with enhanced interactions including a new direct hydrogen bond, water-mediated hydrogen bonds and van der Waals contacts to the 80's loop that are absent in the corresponding wild-type structures. This alternate binding site for P3/P3′ substrate residues is particularly critical for PR fitness when resistance mutations like G48/48′V are present at the flaps. The G48/48′V mutation also alters the binding of P4′ Nle of CA-p2, as well as P3 Thr and P4 Ace residues of p2-NC substrate analogues.

The enhanced binding of CA-p2 and p2-NC substrate analogues with new hydrogen bond interactions observed in PR^{S17} complexes in comparison to PR complexes agrees well with 3.4- and 4.2-fold better K_i values for PR^{S17} relative to those for the wild-type enzyme. In addition, the comparison of PR^{S17} substrate analogue complexes with that of DRV reveals that highly multiple drug-resistant PR^{S17} efficiently binds substrate analogues and DRV with minimal conformational changes, thereby contributing to both viral fitness and drug resistance. The current structural studies of PR^{S17} strongly suggest that G48V mutation plays an important role in the enhanced binding of substrate analogues CA-p2 and p2-NC. Further, the size of the mutated side chain selected at residue 82 may be influenced by the presence of mutation at the flap residue Gly48. In the absence of G48V mutation, Val82 mutations enhance the resistance profile of PR through steric hindrance to inhibitors at the binding site. However, in the presence of G48V flap mutation, mutations of residue 82 to larger side chains like V82F, V82L, and V82I may interfere with the binding of substrates, while smaller V82S and V82A mutations might play a vital role in both enhanced binding of substrate and increased resistance to PIs through the structural shift of 80's loop. The structural features identified in the current studies reveal valuable information for the future design of drugs targeting multidrug-resistant HIV PRs. Clearly, further studies on substrate recognition by multidrug-resistant PR variants will bring out new ways of targeting viral fitness and activity.

MATERIALS AND METHODS

Construction, Expression, and Purification of PR^{S17}. Synthetic genes encoding the 99 amino acid protein named PR^{S17} and its active-site mutant PR^{S17}-D25N (DNA2.0, Menlo Park, CA) were cloned in pJ414 vector flanked by Nde1 and *Bam*HI sites and transformed into *Escherichia coli* BL-21 (DE3, Stratagene). DNA sequencing and electrospray ionization mass spectrometry were used to verify the recombinant construct. Protein expression, purification, and refolding were carried out as described previously.[55,56] In brief, cells were expressed in Luria-Bertani medium and induced with 2 mM isopropyl β-D-1-thiogalactopyranoside. The harvested cells were lysed by the addition of lysozyme (100 μg/mL) and sonication at 4°C. The pelleted inclusion bodies were washed and solubilized in 50 mM Tris−HCL, pH 8.0, 8 M guanidine hydrochloride, 5 mM ethylenediaminetetraacetic acid (EDTA), and 10 mM dithiothreitol. The protein was purified over a Superdex-75 column (HiLoad 2.6 cm × 60 cm, GE HealthCare) under denaturing conditions. The peak fractions were further purified by reverse-phase high-performance liquid chromatography on a SOURCE 15RPC ST 4.6/100 column using AKTA pure chromatography system (GE HealthCare). The purified protein was refolded by extensive dialysis against 30 mM formic acid and concentrated to the desired level using Amicon Ultra concentrators.

Kinetic Inhibition Measurements. Kinetic inhibition values (K_i) of p2-NC and CA-p2 for PR^{S17} were measured using a spectroscopic fluorescence resonance energy-transfer (FRET) substrate analogue of the p2-NC site (H-2992, Bachem, Bubendorf, Switzerland). The peptide sequences of the two substrate analogues are R-V-L-r-F-E-A-Nle for CA-p2 and Ace-T-I-Nle-r-Nle-Q-R p2-NC. Enzyme kinetic parameters k_{cat} and K_m were determined for PR^{S17} using the Michaelis−Menten analysis at 14−180 μM substrate concentration [S]. The k_{cat} and K_m are 69.7 ± 14.4 min^{-1} and 143 ± 33.0 μM, respectively. The k_{cat}/K_m for PR^{S17} of 0.49 ± 0.05 min^{-1} μM^{-1} is comparable to the previously reported values, using a different method (0.55 min^{-1} μM^{-1}).[15] Reactions were performed in a total volume of 100 μL at 37 °C in 50 mM 2-(*N*-morpholino)ethanesulfonic acid pH 5.6, 200 mM sodium chloride, 0.5 mM EDTA, and 2.5% glycerol. Enzyme concentration [E] was 180−370 nM as measured by active-site titration with APV. Inhibition assays used 60 μM [S]. The rate of substrate cleavage under a range of substrate analogue concentrations was measured continuously for 5 min by excitation at 340 nm and emission at 420 nm using a POLARstar OPTIMA microplate reader. The K_i value was determined using the equation $K_i = (IC_{50} - [E]/2)/(1 + [S]/K_m)$. IC_{50} was determined from dose−response curves. K_m values of FRET substrate for PR^{S17} were determined from the Michaelis−Menten analysis at 14−180 μM [S]. All calculations were fitted using Sigmaplot 12.0 (Systat Software Inc., San Jose, CA).

Crystallization. PR^{S17} was complexed with substrate analogues CA-p2 and p2-NC dissolved in dimethyl sulfoxide at a 1:5 molar ratio and incubated on ice for 30 min. The complex was centrifuged at 10 000 rpm for 5 min, and the supernatant was used for crystallization. The crystallization trials were performed at room temperature with the hanging drop vapor diffusion technique. The hanging drop in all crystallization trials was set up with 1 μL of protein solution (5 mg/mL) and 1 μL of reservoir solution. Crystals of inhibitor-free PR^{S17}-D25N were obtained from 1.95 M sodium chloride and 0.1 M bis−Tris pH 7.5. Crystals of PR^{S17}/CA-p2 were grown from reservoir solution containing 2.1 M sodium chloride and 0.1 M 4-(2-hydroxyethyl)-1-piperazineethanesulfonic acid at pH 7.6. The PR^{S17} crystals in complex with substrate analogue p2-NC were obtained in two different space groups $P4_1$ and $P6_1$. The well solution used for growing $PR^{S17\text{-}P41}$/p2-NC crystals was 29.5% poly(ethylene glycol) 4000, 0.2 M ammonium acetate, and 0.1 M sodium acetate buffer at pH 4.6. The $PR^{S17\text{-}P61}$/p2-NC crystals were grown from 35% Tacsimate, pH 7.0 (Hampton Research Corp., Aliso Viejo, CA). Tacsimate contains 1.83 M malonic acid, 0.25 M ammonium citrate tribasic, 0.12 M succinic acid, 0.3 M DL-malic acid, 0.4 M sodium acetate trihydrate, 0.5 M sodium formate, and 0.16 M ammonium tartrate dibasic. Crystals of the wild-type PR/CA-p2 were obtained from 1 M sodium chloride and 0.1 M sodium acetate at pH 4.8. The crystals were cryo-cooled with cryoprotectant containing the respective mother liquor together with 30% glycerol.

X-ray Data Collection and Structure Determination. X-ray diffraction data were collected at 100 K on beamline 22-ID of the Southeast Regional Collaborative Access Team (SER-CAT) at the Advanced Photon Source, Argonne

DOI: 10.1021/acsomega.9b00683
ACS Omega 2019, 4, 8707−8719

National Laboratory. The data were integrated and scaled with HKL2000.[57] The crystal structures of PR^{S17} active-site mutant PR^{S17}-D25N and the substrate analogue complexes PR/CA-p2, PR^{S17}/CA-p2, $PR^{S17\text{-}P41}$/p2-NC, and $PR^{S17\text{-}P61}$/p2-NC were solved by molecular replacement using PHASER.[58,59] The previously solved crystal structure of active PR^{S17} (5T2E)[16] was used as the starting model for PR^{S17} active-site mutant PR^{S17}-D25N. For PR/CA-p2 substrate analogue complex, the crystal structure of PR/p2-NC[24] (2AOD) was used as the starting model. For PR^{S17}/CA-p2 substrate analogue complex, the crystal structure of PR^{S17} complex with darunavir (DRV)[16] (5T2Z) was used as the initial model. Crystal structure of multiple mutants V6 in complex with indinavir (1SGU)[60] was used to solve both PR^{S17}/p2-NC complexes. The PR/CA-p2 complex was refined with SHELX-1997.[61] The PR^{S17}/CA-p2 complex was refined using REFMAC,[62] while the PR^{S17}-D25N and PR^{S17}/p2-NC complexes were initially refined by SHELX-2014[63] and switched to REFMAC during later cycles of refinement. COOT[64] was used for most model building except O[65] was applied for PR/CA-p2. In the PR^{S17}/p2-NC complexes, mutations were added to the model based on the primary sequence and difference density maps. The substrate analogues were fitted into unambiguous electron density in the four complex structures. Solvent molecules were inserted at stereochemically reasonable positions using $2F_o-F_c$ and F_o-F_c maps at 1σ and 3σ levels, respectively. Molecular figures were prepared with PyMOL (http://www.pymol.org).

■ ASSOCIATED CONTENT

Accession Codes

Coordinates and structure factors for the crystal structures PR/CA-p2 (6O48), PR^{S17}-D25N (6O54), PR^{S17}/CA-p2 (6O5X), $PR^{S17\text{-}P41}$/p2-NC (6O57), and $PR^{S17\text{-}P61}$/p2-NC (6O5A) have been deposited in the Protein Data Bank.

■ AUTHOR INFORMATION

Corresponding Author

*E-mail: iweber@gsu.edu.

ORCID

Irene T. Weber: 0000-0003-4876-7393

Funding

The research was supported in part by the National Institute of Health grant GM062920 (I.T.W. and R.W.H.).

Notes

The authors declare no competing financial interest.

■ ACKNOWLEDGMENTS

The authors thank the staff at the Southeast Regional Collaborative Access Team (SER-CAT) at the Advanced Photon Source, Argonne National Laboratory, for assistance during X-ray data collection. Supporting institutions may be found at http://www.ser-cat.org/members.html. Use of the Advanced Photon Source was supported by the U.S. Department of Energy, Office of Science, Office of Basic Energy Sciences, under Contract No. W-31-109-Eng-38.

■ REFERENCES

(1) Deeks, S. G.; Lewin, S. R.; Ross, A. L.; Ananworanich, J.; Benkirane, M.; Cannon, P.; Chomont, N.; Douek, D.; Lifson, J. D.; Lo, Y. R.; Kuritzkes, D.; Margolis, D.; Mellors, J.; Persaud, D.; Tucker, J. D.; Barre-Sinoussi, F.; Alter, G.; Auerbach, J.; Autran, B.; Barouch, D. H.; Behrens, G.; Cavazzana, M.; Chen, Z.; Cohen, E. A.; Corbelli, G. M.; Eholie, S.; Eyal, N.; Fidler, S.; Garcia, L.; Grossman, C.; Henderson, G.; Henrich, T. J.; Jefferys, R.; Kiem, H. P.; McCune, J.; Moodley, K.; Newman, P. A.; Nijhuis, M.; Nsubuga, M. S.; Ott, M.; Palmer, S.; Richman, D.; Saez-Cirion, A.; Sharp, M.; Siliciano, J.; Silvestri, G.; Singh, J.; Spire, B.; Taylor, J.; Tolstrup, M.; Valente, S.; van Lunzen, J.; Walensky, R.; Wilson, I.; Zack, J. International AIDS Society global scientific strategy: towards an HIV cure 2016. *Nat. Med.* **2016**, *22*, 839−850.

(2) Ghosh, A. K.; Osswald, H. L.; Prato, G. Recent Progress in the Development of HIV-1 Protease Inhibitors for the Treatment of HIV/AIDS. *J. Med. Chem.* **2016**, *59*, 5172−5208.

(3) Piot, P.; Abdool Karim, S. S.; Hecht, R.; Legido-Quigley, H.; Buse, K.; Stover, J.; Resch, S.; Ryckman, T.; Mogedal, S.; Dybul, M.; Goosby, E.; Watts, C.; Kilonzo, N.; McManus, J.; Sidibe, M. Defeating AIDS–advancing global health. *Lancet* **2015**, *386*, 171−218.

(4) Weber, I. T.; Agniswamy, J. HIV-1 Protease: Structural Perspectives on Drug Resistance. *Viruses* **2009**, *1*, 1110−1136.

(5) Hyland, L. J.; Tomaszek, T. A., Jr.; Roberts, G. D.; Carr, S. A.; Magaard, V. W.; Bryan, H. L.; Fakhoury, S. A.; Moore, M. L.; Minnich, M. D.; Culp, J. S.; et al. Human immunodeficiency virus-1 protease. 1. Initial velocity studies and kinetic characterization of reaction intermediates by 18O isotope exchange. *Biochemistry* **1991**, *30*, 8441−8453.

(6) Shen, C. H.; Tie, Y.; Yu, X.; Wang, Y. F.; Kovalevsky, A. Y.; Harrison, R. W.; Weber, I. T. Capturing the reaction pathway in near-atomic-resolution crystal structures of HIV-1 protease. *Biochemistry* **2012**, *51*, 7726−7732.

(7) Brik, A.; Wong, C. H. HIV-1 protease: mechanism and drug discovery. *Org. Biomol. Chem.* **2003**, *1*, 5−14.

(8) Hue, S.; Gifford, R. J.; Dunn, D.; Fernhill, E.; Pillay, D. Demonstration of sustained drug-resistant human immunodeficiency virus type 1 lineages circulating among treatment-naive individuals. *J. Virol.* **2009**, *83*, 2645−2654.

(9) Wensing, A. M.; Calvez, V.; Gunthard, H. F.; Johnson, V. A.; Paredes, R.; Pillay, D.; Shafer, R. W.; Richman, D. D. 2017 Update of the Drug Resistance Mutations in HIV-1. *Top. Antiviral Med.* **2017**, *24*, 132−133.

(10) Weber, I. T.; Kneller, D. W.; Wong-Sam, A. Highly resistant HIV-1 proteases and strategies for their inhibition. *Future Med. Chem.* **2015**, *7*, 1023−1038.

(11) Babrzadeh, F.; Varghese, V.; Pacold, M.; Liu, T. F.; Nyren, P.; Schiffer, C.; Fessel, W. J.; Shafer, R. W. Collinearity of protease mutations in HIV-1 samples with high-level protease inhibitor class resistance. *J. Antimicrob. Chemother.* **2013**, *68*, 414−418.

(12) Yu, X.; Weber, I. T.; Harrison, R. W. In *Sparse Representation for Prediction of HIV-1 Protease Drug Resistance*, Proceedings of the 2013 SIAM International Conference on Data Mining; SIAM, 2013; pp 342−349.

(13) Yu, X.; Weber, I. T.; Harrison, R. W. Prediction of HIV drug resistance from genotype with encoded three-dimensional protein structure. *BMC Genomics* **2014**, *15*, S1.

(14) Yu, X.; Weber, I. T.; Harrison, R. W. Identifying representative drug resistant mutants of HIV. *BMC Bioinf.* **2015**, *16*, S1.

(15) Park, J. H.; Sayer, J. M.; Aniana, A.; Yu, X.; Weber, I. T.; Harrison, R. W.; Louis, J. M. Binding of clinical inhibitors to a model precursor of a rationally selected multidrug resistant HIV-1 protease is significantly weaker than to the released mature enzyme. *Biochemistry* **2016**, *55*, 2390−2400.

(16) Agniswamy, J.; Louis, J. M.; Roche, J.; Harrison, R. W.; Weber, I. T. Structural Studies of a Rationally Selected Multi-Drug Resistant HIV-1 Protease Reveal Synergistic Effect of Distal Mutations on Flap Dynamics. *PLoS One* **2016**, *11*, No. e0168616.

(17) Agniswamy, J.; Shen, C. H.; Aniana, A.; Sayer, J. M.; Louis, J. M.; Weber, I. T. HIV-1 Protease with 20 Mutations Exhibits Extreme Resistance to Clinical Inhibitors through Coordinated Structural Rearrangements. *Biochemistry* **2012**, *51*, 2819−2828.

(18) Martin, P.; Vickrey, J. F.; Proteasa, G.; Jimenez, Y. L.; Wawrzak, Z.; Winters, M. A.; Merigan, T. C.; Kovari, L. C. "Wide-open" 1.3 A

DOI: 10.1021/acsomega.9b00683
ACS Omega 2019, 4, 8707−8719

structure of a multidrug-resistant HIV-1 protease as a drug target. *Structure* **2005**, *13*, 1887−1895.
(19) Perryman, A. L.; Lin, J. H.; McCammon, J. A. HIV-1 protease molecular dynamics of a wild-type and of the V82F/I84V mutant: possible contributions to drug resistance and a potential new target site for drugs. *Protein Sci.* **2004**, *13*, 1108−1123.
(20) Pettit, S. C.; Moody, M. D.; Wehbie, R. S.; Kaplan, A. H.; Nantermet, P. V.; Klein, C. A.; Swanstrom, R. The p2 domain of human immunodeficiency virus type 1 Gag regulates sequential proteolytic processing and is required to produce fully infectious virions. *J. Virol.* **1994**, *68*, 8017−8027.
(21) Kožíšek, M.; Henke, S.; Šašková, K. G.; Jacobs, G. B.; Schuch, A.; Buchholz, B.; Müller, V.; Krräusslich, H. G.; Řezáčová, P.; Konvalinka, J.; Bodem, J. Mutations in HIV-1 gag and pol compensate for the loss of viral fitness caused by a highly mutated protease. *Antimicrob. Agents Chemother.* **2012**, *56*, 4320−4330.
(22) Tomasselli, A. G.; Olsen, M. K.; Hui, J. O.; Staples, D. J.; Sawyer, T. K.; Heinrikson, R. L.; Tomich, C. S. Substrate analogue inhibition and active site titration of purified recombinant HIV-1 protease. *Biochemistry* **1990**, *29*, 264−269.
(23) Tözsér, J.; Bláha, I.; Copeland, T. D.; Wondrak, E. M.; Oroszlan, S. Comparison of the HIV-1 and HIV-2 proteinases using oligopeptide substrates representing cleavage sites in Gag and Gag-Pol polyproteins. *FEBS Lett.* **1991**, *281*, 77−80.
(24) Tie, Y.; Boross, P. I.; Wang, Y. F.; Gaddis, L.; Liu, F.; Chen, X.; Tozser, J.; Harrison, R. W.; Weber, I. T. Molecular basis for substrate recognition and drug resistance from 1.1 to 1.6 angstroms resolution crystal structures of HIV-1 protease mutants with substrate analogs. *FEBS J.* **2005**, *272*, 5265−5277.
(25) Yedidi, R. S.; Proteasa, G.; Martinez, J. L.; Vickrey, J. F.; Martin, P. D.; Wawrzak, Z.; Liu, Z.; Kovari, I. A.; Kovari, L. C. Contribution of the 80s loop of HIV-1 protease to the multidrug-resistance mechanism: crystallographic study of MDR769 HIV-1 protease variants. *Acta Crystallogr., Sect. D: Biol. Crystallogr.* **2011**, *67*, 524−532.
(26) Liu, F.; Kovalevsky, A. Y.; Tie, Y.; Ghosh, A. K.; Harrison, R. W.; Weber, I. T. Effect of flap mutations on structure of HIV-1 protease and inhibition by saquinavir and darunavir. *J. Mol. Biol.* **2008**, *381*, 102−115.
(27) Kovalevsky, A. Y.; Liu, F.; Leshchenko, S.; Ghosh, A. K.; Louis, J. M.; Harrison, R. W.; Weber, I. T. Ultra-high resolution crystal structure of HIV-1 protease mutant reveals two binding sites for clinical inhibitor TMC114. *J. Mol. Biol.* **2006**, *363*, 161−173.
(28) Wlodawer, A.; Miller, M.; Jaskolski, M.; Sathyanarayana, B. K.; Baldwin, E.; Weber, I. T.; Selk, L. M.; Clawson, L.; Schneider, J.; Kent, S. B. Conserved folding in retroviral proteases: crystal structure of a synthetic HIV-1 protease. *Science* **1989**, *245*, 616−621.
(29) Shafer, R. W. Rationale and uses of a public HIV drug-resistance database. *J. Infect. Dis.* **2006**, *194*, S51−S58.
(30) Chen, J.; Wang, X.; Zhu, T.; Zhang, Q.; Zhang, J. Z. A Comparative Insight into Amprenavir Resistance of Mutations V32I, G48V, I50V, I54V, and I84V in HIV-1 Protease Based on Thermodynamic Integration and MM-PBSA Methods. *J. Chem. Inf. Model.* **2015**, *55*, 1903−1913.
(31) Shafer, R. W.; Stevenson, D.; Chan, B. Human Immunodeficiency Virus Reverse Transcriptase and Protease Sequence Database. *Nucleic Acids Res.* **1999**, *27*, 348−352.
(32) Gulnik, S. V.; Suvorov, L. I.; Liu, B.; Yu, B.; Anderson, B.; Mitsuya, H.; Erickson, J. W. Kinetic characterization and cross-resistance patterns of HIV-1 protease mutants selected under drug pressure. *Biochemistry* **1995**, *34*, 9282−9287.
(33) Klabe, R. M.; Bacheler, L. T.; Ala, P. J.; Erickson-Viitanen, S.; Meek, J. L. Resistance to HIV protease inhibitors: a comparison of enzyme inhibition and antiviral potency. *Biochemistry* **1998**, *37*, 8735−8742.
(34) Mahalingam, B.; Wang, Y. F.; Boross, P. I.; Tozser, J.; Louis, J. M.; Harrison, R. W.; Weber, I. T. Crystal structures of HIV protease V82A and L90M mutants reveal changes in the indinavir-binding site. *Eur. J. Biochem.* **2004**, *271*, 1516−1524.
(35) Tie, Y.; Boross, P. I.; Wang, Y. F.; Gaddis, L.; Hussain, A. K.; Leshchenko, S.; Ghosh, A. K.; Louis, J. M.; Harrison, R. W.; Weber, I. T. High resolution crystal structures of HIV-1 protease with a potent non-peptide inhibitor (UIC-94017) active against multi-drug-resistant clinical strains. *J. Mol. Biol.* **2004**, *338*, 341−352.
(36) Agniswamy, J.; Weber, I. T. HIV-1 protease: structural prespectives on drug resistance. *Viruses* **2009**, *1*, 1110−1136.
(37) Kempf, D. J.; Marsh, K. C.; Denissen, J. F.; McDonald, E.; Vasavanonda, S.; Flentge, C. A.; Green, B. E.; Fino, L.; Park, C. H.; Kong, X. P.; et al. ABT-538 is a potent inhibitor of human immunodeficiency virus protease and has high oral bioavailability in humans. *Proc. Natl. Acad. Sci. U.S.A.* **1995**, *92*, 2484−2488.
(38) Prabu-Jeyabalan, M.; Nalivaika, E. A.; King, N. M.; Schiffer, C. A. Viability of a drug-resistant human immunodeficiency virus type 1 protease variant: structural insights for better antiviral therapy. *J. Virol.* **2003**, *77*, 1306−1315.
(39) Dam, E.; Quercia, R.; Glass, B.; Descamps, D.; Launay, O.; Duval, X.; Krausslich, H. G.; Hance, A. J.; Clavel, F. Gag mutations strongly contribute to HIV-1 resistance to protease inhibitors in highly drug-experienced patients besides compensating for fitness loss. *PLoS Pathog.* **2009**, *5*, No. e1000345.
(40) Bally, F.; Martinez, R.; Peters, S.; Sudre, P.; Telenti, A. Polymorphism of HIV type 1 gag p7/p1 and p1/p6 cleavage sites: clinical significance and implications for resistance to protease inhibitors. *AIDS Res. Hum. Retroviruses* **2000**, *16*, 1209−1213.
(41) Fehér, A.; Weber, I. T.; Bagossi, P.; Boross, P.; Mahalingam, B.; Louis, J. M.; Copeland, T. D.; Torshin, I. Y.; Harrison, R. W.; Tözsér, J. Effect of sequence polymorphism and drug resistance on two HIV-1 Gag processing sites. *Eur. J. Biochem.* **2002**, *269*, 4114−4120.
(42) Mammano, F.; Petit, C.; Clavel, F. Resistance-associated loss of viral fitness in human immunodeficiency virus type 1: phenotypic analysis of protease and gag coevolution in protease inhibitor-treated patients. *J. Virol.* **1998**, *72*, 7632−7637.
(43) Pettit, S. C.; Sheng, N.; Tritch, R.; Erickson-Viitanen, S.; Swanstrom, R. The Regulation of Sequential Processing of HIV-1 Gag by the Viral Protease. In *Aspartic Proteinases*; James, M. N. G., Ed.; Advances in Experimental Medicine and Biology; Springer: Boston, MA, 1998; Vol. *436*, pp 15−25.
(44) La Seta Catamancio, S.; De Pasquale, M. P.; Citterio, P.; Kurtagic, S.; Galli, M.; Rusconi, S. In vitro evolution of the human immunodeficiency virus type 1 gag-protease region and maintenance of reverse transcriptase resistance following prolonged drug exposure. *J. Clin. Microbiol.* **2001**, *39*, 1124−1129.
(45) Prabu-Jeyabalan, M.; Nalivaika, E. A.; King, N. M.; Schiffer, C. A. Structural basis for coevolution of a human immunodeficiency virus type 1 nucleocapsid-p1 cleavage site with a V82A drug-resistant mutation in viral protease. *J. Virol.* **2004**, *78*, 12446−12454.
(46) Rhee, S. Y.; Taylor, J.; Fessel, W. J.; Kaufman, D.; Towner, W.; Troia, P.; Ruane, P.; Hellinger, J.; Shirvani, V.; Zolopa, A.; Shafer, R. W. HIV-1 protease mutations and protease inhibitor cross-resistance. *Antimicrob. Agents Chemother.* **2010**, *54*, 4253−4261.
(47) Kantor, R.; Fessel, W. J.; Zolopa, A. R.; Israelski, D.; Shulman, N.; Montoya, J. G.; Harbour, M.; Schapiro, J. M.; Shafer, R. W. Evolution of primary protease inhibitor resistance mutations during protease inhibitor salvage therapy. *Antimicrob. Agents Chemother.* **2002**, *46*, 1086−1092.
(48) Clemente, J. C.; Coman, R. M.; Thiaville, M. M.; Janka, L. K.; Jeung, J. A.; Nukoolkarn, S.; Govindasamy, L.; Agbandje-McKenna, M.; McKenna, R.; Leelamanit, W.; Goodenow, M. M.; Dunn, B. M. Analysis of HIV-1 CRF_01 A/E protease inhibitor resistance: structural determinants for maintaining sensitivity and developing resistance to atazanavir. *Biochemistry* **2006**, *45*, 5468−5477.
(49) Shahriar, R.; Rhee, S. Y.; Liu, T. F.; Fessel, W. J.; Scarsella, A.; Towner, W.; Holmes, S. P.; Zolopa, A. R.; Shafer, R. W. Nonpolymorphic human immunodeficiency virus type 1 protease and reverse transcriptase treatment-selected mutations. *Antimicrob. Agents Chemother.* **2009**, *53*, 4869−4878.
(50) Svicher, V.; Ceccherini-Silberstein, F.; Erba, F.; Santoro, M.; Gori, C.; Bellocchi, M. C.; Giannella, S.; Trotta, M. P.; Monforte, A.;

DOI: 10.1021/acsomega.9b00683
ACS Omega 2019, 4, 8707−8719

Antinori, A.; Perno, C. F. Novel human immunodeficiency virus type 1 protease mutations potentially involved in resistance to protease inhibitors. *Antimicrob. Agents Chemother.* **2005**, *49*, 2015−2025.
(51) Prashar, V.; Bihani, S. C.; Das, A.; Rao, D. R.; Hosur, M. V. Insights into the mechanism of drug resistance: X-ray structure analysis of G48V/C95F tethered HIV-1 protease dimer/saquinavir complex. *Biochem. Biophys. Res. Commun.* **2010**, *396*, 1018−1023.
(52) Boden, D.; Markowitz, M. Resistance to human immunodeficiency virus type 1 protease inhibitors. *Antimicrob. Agents Chemother.* **1998**, *42*, 2775−2783.
(53) Liu, F.; Kovalevsky, A. Y.; Louis, J. M.; Boross, P. I.; Wang, Y. F.; Harrison, R. W.; Weber, I. T. Mechanism of drug resistance revealed by the crystal structure of the unliganded HIV-1 protease with F53L mutation. *J. Mol. Biol.* **2006**, *358*, 1191−1199.
(54) Nakashima, M.; Ode, H.; Suzuki, K.; Fujino, M.; Maejima, M.; Kimura, Y.; Masaoka, T.; Hattori, J.; Matsuda, M.; Hachiya, A.; Yokomaku, Y.; Suzuki, A.; Watanabe, N.; Sugiura, W.; Iwatani, Y. Unique Flap Conformation in an HIV-1 Protease with High-Level Darunavir Resistance. *Front. Microbiol.* **2016**, *7*, 61.
(55) Sayer, J. M.; Agniswamy, J.; Weber, I. T.; Louis, J. M. Autocatalytic maturation, physical/chemical properties, and crystal structure of group N HIV-1 protease: relevance to drug resistance. *Protein Sci.* **2010**, *19*, 2055−2072.
(56) Louis, J. M.; Ishima, R.; Aniana, A.; Sayer, J. M. Revealing the dimer dissociation and existence of a folded monomer of the mature HIV-2 protease. *Protein Sci.* **2009**, *18*, 2442−2453.
(57) Otwinowski, Z.; Minor, W. Processing of X-ray diffraction data collected in oscillation mode. *Method Enzymol.* **1997**, *276*, 307−326.
(58) Storoni, L. C.; McCoy, A. J.; Read, R. J. Likelihood-enhanced fast rotation functions. *Acta Crystallogr., Sect. D: Biol. Crystallogr.* **2004**, *60*, 432−438.
(59) McCoy, A. J.; Grosse-Kunstleve, R. W.; Storoni, L. C.; Read, R. J. Likelihood-enhanced fast translation functions. *Acta Crystallogr., Sect. D: Biol. Crystallogr.* **2005**, *61*, 458−464.
(60) Clemente, J. C.; Moose, R. E.; Hemrajani, R.; Whitford, L. R.; Govindasamy, L.; Reutzel, R.; McKenna, R.; Agbandje-McKenna, M.; Goodenow, M. M.; Dunn, B. M. Comparing the accumulation of active- and nonactive-site mutations in the HIV-1 protease. *Biochemistry* **2004**, *43*, 12141−12151.
(61) Sheldrick, G. M.; Schneider, T. R. SHELXL: high-resolution refinement. *Methods Enzymol.* **1997**, *277*, 319−343.
(62) Murshudov, G. N.; Vagin, A. A.; Dodson, E. J. Refinement of macromolecular structures by the maximum-likelihood method. *Acta Crystallogr., Sect. D: Biol. Crystallogr.* **1997**, *53*, 240−255.
(63) Sheldrick, G. M. Crystal structure refinement with SHELXL. *Acta Crystallogr., Sect. C: Struct. Chem.* **2015**, *71*, 3−8.
(64) Emsley, P.; Cowtan, K. Coot: model-building tools for molecular graphics. *Acta Crystallogr., Sect. D: Biol. Crystallogr.* **2004**, *60*, 2126−2132.
(65) Jones, T. A.; Zou, J. Y.; Cowan, S. W.; Kjeldgaard, M. Improved methods for building protein models in electron density maps and the location of errors in these models. *Acta Crystallogr., Sect. A: Found. Crystallogr.* **1991**, *47*, 110−119.

DOI: 10.1021/acsomega.9b00683
ACS Omega 2019, 4, 8707−8719